CHEMBIOCHEM

DOI: 10.1002/cbic.200800581

Pathogenic Mutations Shift the Equilibria of α-Synuclein Single Molecules towards Structured Conformers

Marco Brucale,[a] Massimo Sandal,[a] Selena Di Maio,[a] Aldo Rampioni,[a] Isabella Tessari,[b] Laura Tosatto,[b] Marco Bisaglia,[b] Luigi Bubacco,[b] and Bruno Samorì*[a]

Dedicated to Professor Roeland Nolte on the occasion of his 65th birthday.

α-synuclein (α-Syn) is an abundant brain protein whose mutations have been linked to early-onset Parkinson's disease (PD). We recently demonstrated, by means of a single-molecule force spectroscopy (SMFS) methodology, that the conformational equilibrium of monomeric wild-type (WT) α-Syn shifts toward β-containing structures in several unrelated conditions linked to PD pathogenicity. Herein, we follow the same methodology previously employed for WT α-Syn to characterize the conformational heterogeneity of pathological α-Syn mutants A30P, A53T, and E46K. Contrary to the bulk ensemble-averaged spectroscopies so far employed to this end by different authors, our single-molecule methodology monitored marked differences in the conformational behaviors of the mutants with respect to the WT sequence. We found that all the mutants have a much higher propensity than the WT to adopt a monomeric compact conformation that is compatible with the acquiring of β structure. Mutants A30P and A53T show a similar conformational equilibrium that is significantly different from that of E46K. Another class of conformations, stabilized by mechanically weak interactions (MWI), shows a higher variety in the mutants than in the WT protein. In the A30P mutant these interactions are relatively stronger, and therefore the corresponding conformations are possibly more structured. The more structured and globular conformations of the mutants can explain their higher propensity to aggregate with respect to the WT.

Introduction

The natively disordered protein α-synuclein (α-Syn) is the main constituent of Lewy bodies, which are intracellular proteinaceous inclusion bodies, whose formation is a cellular hallmark of Parkinson's disease (PD) and other neurodegenerative pathologies.[1–3] Although there is a wide consensus in the scientific community that the in vivo aggregation of α-Syn into amyloid fibrils and, eventually, Lewy bodies is a critical step in the onset of PD, the details of this process are largely unknown. In particular, no comprehensive aggregation pathway detailing the role of intermediates is currently available. A better comprehension of the aggregation mechanisms could ultimately be functional in devising strategies aimed at avoiding the onset of PD or mitigating its symptoms.

When reproduced in vitro and investigated by spectroscopic techniques, fibrils of α-Syn found in the dopaminergic neurons of PD patients reveal a high content of β-sheet secondary structure.[4,5] α-Syn is also found to form the same type of fibrils in vitro under a variety of conditions.[3] Since α-Syn is a typical example of natively unfolded protein (NUP),[6] and as such lacks a well-defined three-dimensional structure,[7] the aggregation process is primarily one of acquiring structure.[8] The major steps of the process are the appearance of aggregation-prone species of the monomer, the formation of oligomers, and, eventually, the nucleation and growth of fibrils or other macroscopic aggregates. Different secondary-structure contents were indeed identified in the aggregates at specific stages of the fibrillization process.[9–12] Several aggregation intermediate species with different morphologies and sizes were observed,[10,12,13] some of which were suggested to be extraneous to the fibrillization pathway.[13,14] α-Syn fibrillization is thus a multistep process, with branched reaction pathways that also include dead ends, and involves a number of oligomeric species with different structures and properties.[15] Most importantly, it is not obvious which of the many species formed during the fibrillization process is most dangerous for the organism, although evidence is accumulating that specifically identifies annular, ring-like oligomeric forms as the most toxic.[9,16–18] Conversely, fibril formation could be functional in sequestering the dangerous oligomeric species.[19]

Interestingly, the point-mutated α-synucleins responsible for familial PD, the A30P, A53T, and E46K mutants, have been reported to show marked differences in their aggregation behaviors compared to WT α-Syn, with regard to both fibrillization and oligomerization.[10,17–25] For instance, compared to WT α-Syn, A30P was found to promote the formation of annular, pore-like protofibrils, whereas A53T promotes the formation of

[a] Dr. M. Brucale, Dr. M. Sandal, S. Di Maio, Dr. A. Rampioni, Prof. B. Samorì
Department of Biochemistry, University of Bologna
via Irnerio 48, 40126 Bologna (Italy)
Fax: (+39) 051-2094387
E-mail: bruno.samori@unibo.it

[b] Dr. I. Tessari, L. Tosatto, Dr. M. Bisaglia, Prof. L. Bubacco
Department of Biology, University of Padova
via U. Bassi 58/B, 35121 Padova (Italy)

Supporting information for this article is available on the WWW under http://dx.doi.org/10.1002/cbic.200800581 or from the author.

both annular and tubular protofibrillar structures. In contrast, the E46K mutant reduces the abundance of such aggregates.[18] Wild-type α-Syn was also found to form annular protofibrils, but only after extended incubation.[17] Both E46K and A53T exhibit an increased rate of fibrillization with respect to WT α-Syn,[21,26] whereas the A30P mutant either does not display such increase[19,24] or even shows a decrease.[25]

Quite surprisingly, in ensemble-averaged experiments, such marked contrasts in the aggregation behavior of the different mutants have not been found to correspond to analogously clear-cut differences in their monomeric conformational behavior.[19,27] When they were studied by means of various spectroscopic techniques, only subtle differences were detected at the monomeric level between WT, A30P, A53T, and E46K α-Syn in terms of amount of non-Aβ component (NAC) region shielding,[28,29] N-terminal α-helix propensity,[27] and β-structure propensity at high concentration.[20]

Recently, we described a SMFS methodology that makes it possible to show that monomeric α-Syn is capable of assuming multiple, but discrete, structured conformations prior to any aggregation step.[30] We identified three classes of mechanically different monomeric α-Syn conformations, one of which is compatible with an amount of β-structuring similar to that found in α-Syn aggregates. Using this methodology, we could quantify the population of these classes of α-Syn conformations, and how their relative abundance shifts in response to different environments. In particular, the proportion of β-containing conformations increased markedly under conditions known to be related to PD pathogenesis. This result suggests that the specific ensemble of conformations visited by α-Syn at the monomeric level, and their relative abundance, can influence the whole aggregation process right at the onset. We thus employed the same SMFS methodology mentioned above to characterize the conformational equilibria of monomeric α-Syn pathological mutants A30P, A53T, and E46K, and evaluate the differences with respect to WT and between each other.

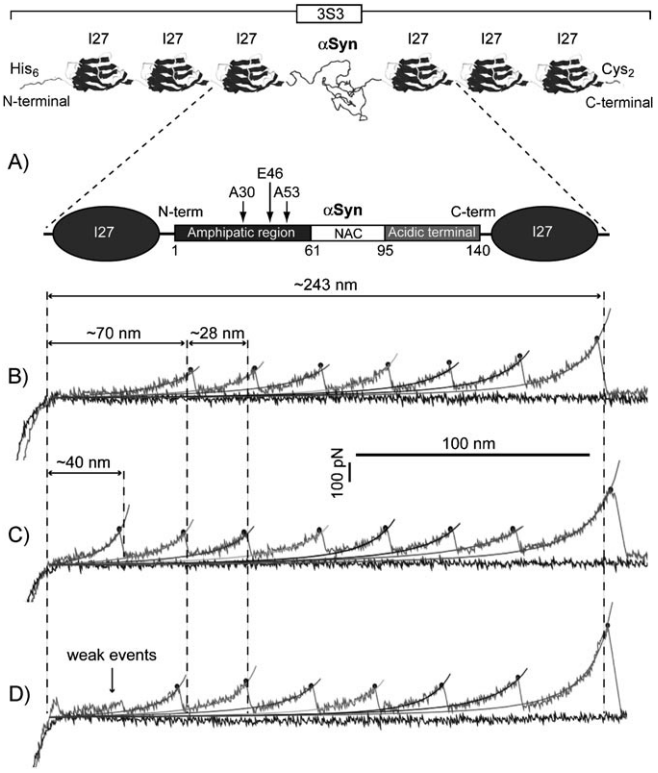

Figure 1. A) Schematic representation of the polyprotein 3S3 constructs containing the α-Syn sequence flanked on either side by three titin I27 modules, the N-terminal His-tag needed for purification purposes, and the C-terminal Cys–Cys tail needed for covalent attachment to the gold surface. In the α-Syn moiety (enlarged), three regions are shown: 1) the amphipathic region, prone to fold into α-helical structures when in contact with phospholipid membranes; 2) the fibrillogenic NAC region, characteristic of the fibril core of α-Syn amyloids; and 3) the acidic C-terminal tail, strongly charged and not prone to fold. The positions of mutation sites A30, E46, and A53 are indicated. B) Example of a curve characterized by a featureless region assigned to the stretching of α-Syn moiety having the mechanical properties of a random coil (see Results). This region is followed (from left to right) by six unfolding peaks ~200 pN high, with ~28 nm gaps between each, assigned to the unfolding of the I27 domains. The characteristic contour lengths of the fully folded construct, of the I27 modules and of the wholly unfolded construct are shown (dashed lines). In all cases, contour lengths were obtained by fitting a worm-like chain equation with two free parameters (contour and persistence length). C) Example of the curves featuring the β-like signature of α-Syn (see Results), showing seven practically indistinguishable unfolding events of similar magnitude and spacing. D) Example of the curves featuring the signature of mechanically weak interactions, showing small peaks preceding the six saw-tooth-like peaks.

Results

A chimeric polyprotein construct for mechanical unfolding SMFS experiments

The SMFS methodology we employed in this study has been described elsewhere.[30] Briefly, chimeric polyproteins composed of a single α-Syn module flanked on either side by three tandem I27 domains (Figure 1 A, 3S3) were expressed. Two cysteines were added at the C-terminal to promote binding to gold surfaces (see the Experimental section). The central α-Syn module had the sequence of either WT α-Syn or one of its pathogenic mutations, A30P, A53T, or E46K, to give a total of four different chimeric 3S3 constructs. Flanking I27 domains act both as "molecular handles" and as an internal mechanical gauge that allows the unambiguous recognition of SMFS signals originating only from single molecules. Polyprotein constructs were allowed to deposit on a gold surface at a concentration of ~100 μg mL^{-1}. For more details on the SMFS experimental approach please refer to the many excellent research articles and reviews available in the literature, focusing on many diverse aspects of SMFS experiments performed on chimeric polyproteins.[31–48]

Tens of thousands of force versus extension curves were recorded on an atomic force microscopy (AFM) apparatus for each construct, only a fraction of which contained single-molecule mechanical unfolding information. After automatic data filtering, only those traces that could be unambiguously assigned to the complete mechanical unfolding of single 3S3 molecules were tagged for successive measurement, while the rest were discarded. (See the Experimental Section for a detailed explanation of the employed data-filtering criteria).

The remaining curves were then examined and characterized in terms of position, height, and number of their mechanical unfolding peaks. (See the Experimental Section for details on data processing, and the Supporting Information for complete contour length and rupture force data.) It must be emphasized that the contour-length increase caused by each rupture event allows the span of the amino acid chain that was involved in that interaction to be univocally quantified. This analysis evidenced only three homogeneous classes of curves (Figure 1 B–D), revealing thus that α-Syn is capable of assuming only three mechanically distinct groups of conformations in the 3S3 construct. Unfolding curves of 3S3 constructs containing WT or point-mutated α-Syn, collected under the same experimental conditions, showed a characteristic distribution of the relative population of the three conformations (see Figure 2 A), thus revealing that the point mutations have a significant impact on the monomeric α-Syn conformational equilibrium.

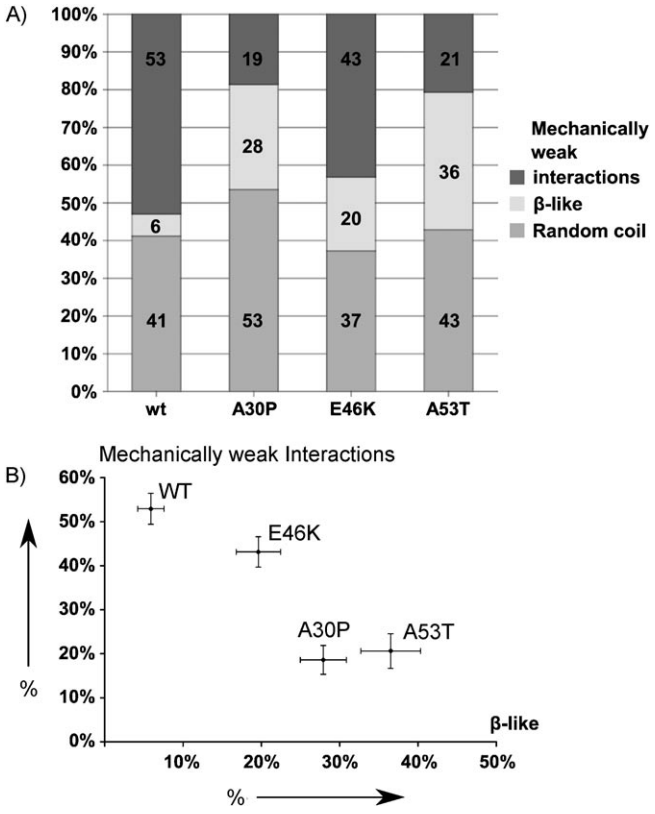

Figure 2. A) Population of α-Syn conformers in the four α-Syn sequence variants tested in this work. Percentages observed for each curve type (see Figure 1) of the wild-type protein ($n=51$), the A30P mutant ($n=43$), the E46K mutant ($n=51$), and the A53T mutant ($n=63$) B) Graph showing the marked dissimilarity between WT α-Syn and the three pathogenic mutants examined in this study. Error bars show standard deviations.

Three classes of mechanical behavior

The present division into classes follows the one we described in ref. [30]. One homogeneous group of curves showed six unfolding peaks, evenly spaced by a distance corresponding to the unfolding of an I27 module (Figure 1 B). In these curves, the average contour length measured at the first I27 unfolding peak was 68 ± 15 nm, corresponding to that of a fully stretched α-Syn moiety (49 nm) plus six folded I27 modules (ca. 4–4.5 nm each).[49] This means that in these curves, α-Syn was captured in a conformation whose extension does not imply the overcoming of measurable unfolding energy barriers, that is, that offered a purely entropic mechanical resistance to pulling. This is a typical behavior of random coils or mostly unfolded conformations. Thus, we assign this class to mainly unfolded α-Syn monomer conformations. See Figures S1, S5 A and S7 in the Supporting Information for a more detailed characterization of this class of curves.

Another highly homogeneous group of curves showed seven equally spaced peaks (Figure 1 C). The average contour length measured at the second peak was 70 ± 10 nm, in good accord with the value found at the first I27 peak in the class of curves with six peaks described above. The seventh peak appears in the region that contains no signal when α-Syn is in random coil. This does not imply that the first peak in these curves can be ascribed to the unfolding of α-Syn, but rather, that one of the seven peaks must necessarily be due to the mechanical unfolding of an α-Syn compact conformation, since significant mechanical resistance is recorded at elongations that are smaller than a fully stretched α-Syn. Thus, in these curves α-Syn was captured in a conformation that offers a high mechanical resistance to pulling, comparable to that of I27 modules. The only secondary structural motif known to be capable of showing such high unfolding forces is the antiparallel β-sheet, so we assign this class of curves to β-rich α-Syn conformations. In these curves, the average contour length of the first peak is only 40 ± 7 nm, which corresponds (after subtracting the length of six folded I27 domains) to a synuclein free chain of ~50 amino acids (aa) and, consequently, an α-Syn folded domain of about 90 aa. Interestingly, this length matches the portion of α-Syn that is found to be included in the fibrils after aggregation.[4,12] See Figures S2, S5B and S6 for a more detailed characterization of this class of curves.

It is important to note that the occurrence of a seventh peak in the class of curves described above cannot be attributed to the unfolding of additional I27 domains in dimerized 3S3 constructs. First and foremost, a control experiment performed on WT 3S3 under disulfide-reducing conditions[30] showed the same occurrence of seven-peaked curves as in the experiments conducted without the addition of a reducing agent.

Under nonreducing conditions, 3S3 can form dimers, and we indeed observed an extremely small proportion of curves (i.e., about 0.002% of the recorded curves) attributable to the mechanical stretching of such molecules. However, these force traces could be easily distinguished from those generated by the unfolding of a monomeric 3S3 construct, and thus discarded. Most importantly, no geometry of pulling of a 3S3–3S3 dimer can give seven-peaked force traces like those described above. If one such dimer were indeed picked up in a position that resulted in exactly seven I27 modules being trapped between the AFM tip and the surface, then at least one α-Syn moiety would necessarily also be included. For this reason, the resulting force trace would inevitably show a distance between

the first I27 peak and the contact point equal to or longer than the length of a fully extended α-Syn molecule. Since the first peaks in the class of seven-peaked curves consistently show a contour length of 40 ± 7 nm, this can only be ascribed to the unfolding of seven adjacent modules, one of which must necessarily be α-Syn. See Figure S4 for an example of a force trace showing the mechanical unfolding of a 3S3–3S3 dimer.

The possibility exists for a 3S3 construct in which α-Syn is in a compact, "β-rich" conformation to be picked up by the AFM tip at a position that would result in a mechanical unfolding trace showing only six peaks. However, in this case, the contour length of the first peak would not be equal to a fully stretched α-Syn plus six folded I27 modules, as in the first class of curves described above. Rather, it would be significantly shorter. The total construct length at detachment would also be noticeably shorter. An exhaustive report on the implications of this observation is included in the Supporting Information (Figures S3 and S7B).

Other types of signal artifacts, such as the AFM tip's simultaneously pulling more than one 3S3 construct, can also be cogently ruled out, as discussed elsewhere.[30]

Finally, curves not assignable to the previous two classes were grouped in a third class. In all these curves, weak mechanical signals appeared between the first I27 peak and the contact point (see, e.g., Figure 1D) signifying that α-Syn was captured in conformations stabilized by interactions that offered a limited mechanical resistance to unfolding (henceforward called "Mechanically Weak Interactions", MWIs). Similarly to what was found in the previously described classes of curves, the distance between the first I27 unfolding peak and contact point is 73 ± 13 nm, corresponding to the length of the totally unfolded α-Syn plus six folded I27 modules. The positions and rupture forces of the MWI appearing in this class of curves show an higher degree of diversity with respect to all other signals (Figure 3; see Figure S8 for a more detailed characterization of this class of curves).

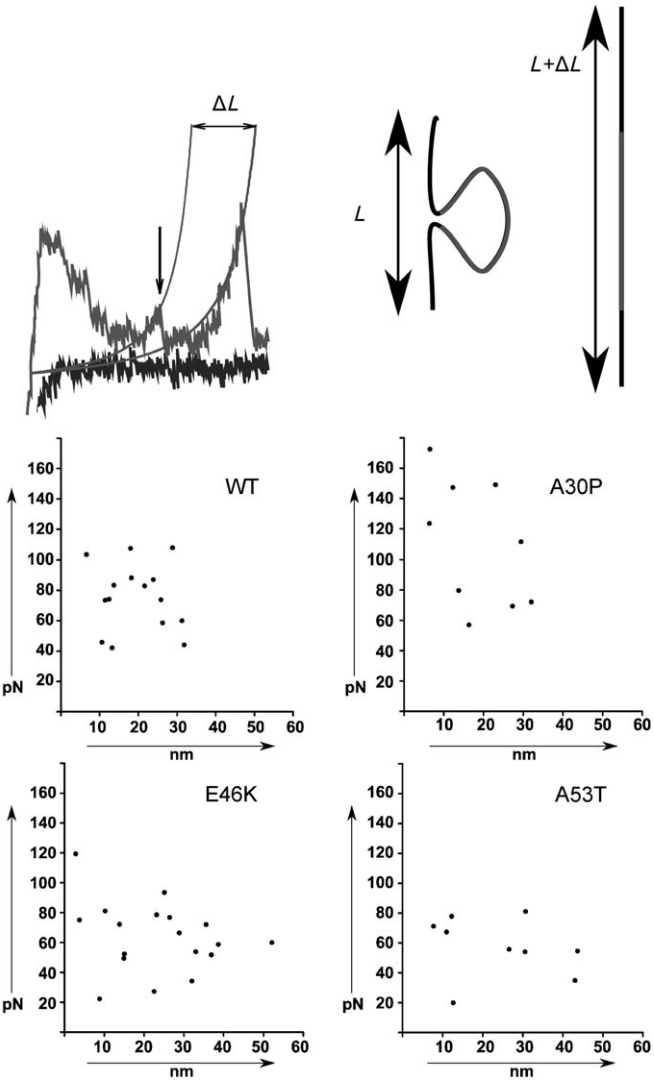

Figure 3. Top: The measurement of MWI interaction lengths. A worm-like chain function (see the Experimental Section) is fitted to the MWI peak and the first I27 unfolding peak. The difference between the asymptote lengths gives the contour length of the loop enclosed by the MWI. Bottom: Scatter plots showing the size of loops enclosed by MWIs versus the corresponding measured interaction force for each of the four α-Syn sequence variants.

Mutations affect the conformational equilibria of the α-Syn variant moieties in the 3S3 constructs

As shown in Figure 2, all three mutants show a markedly higher proportion of β structure than WT α-Syn, which was observed to have a β conformation in only 6 ± 2% of the curves. A53T shows the largest β-structure propensity (36 ± 4%) while A30P and E46K have lower values (28 ± 3% and 20 ± 3% respectively).

The opposite is observed for curves containing MWI-related weak unfolding events: WT α-Syn has the highest value (53 ± 4%), and all mutants show significantly lower percentages. A30P and A53T have very similar values and are the most different from WT α-Syn (19 ± 3% and 21 ± 3% respectively), while E46K shows an intermediate value (43 ± 4%). For each 3S3 variant, the percentage of curves showing the rupture of the MWIs that stabilize the α-Syn moiety was plotted against the percentage of those corresponding to the unfolding of α-Syn β structured conformers (Figure 2B). An anticorrelation between the two populations is clearly shown by the plot

The abundance of random-coil-extended conformations is very similar for WT, E46K, and A53T (41 ± 4%, 36 ± 3%, and 43 ± 4%, respectively), while it is higher for A30P (53 ± 3%). Remarkably, the ratio between β-structured and random-coil conformers is roughly similar for all three mutants (0.5 ± 0.1, 0.5 ± 0.1, and 0.8 ± 0.2 for A30P, E46K, and A53T respectively), while it is markedly lower for WT 3S3 (0.15 ± 0.05)

Mutations in the 3S3 construct widen the variety of MWI

The profiles of the force curves corresponding to α-Syn in a random-coil conformation and in the compact β structures were extremely homogeneous and showed no significant differences among WT α-Syn and mutants, apart from their rela-

tive abundance; this suggests a unique structure for all sequence variants. In contrast, mechanically weak signals showed a higher variety among the different α-Syn species. The distances between the MWI signal and the contact point correspond to the 3S3 chain length that is already accessible to extension prior to the mechanical rupture of the MWI. Accordingly, the distance between the MWI signal and the first I27 unfolding peak corresponds to the 3S3 chain length, which was rendered accessible to extension by the rupture of the same MWI. This length, that is the length of the loop enclosed by each MWI, was plotted against the corresponding rupture force (Figure 3). The MWI scatter plot of WT α-Syn shows that all weak peaks have a rupture force below ~100 pN, and their distance from the contact point does not exceed ~30 nm. Conversely, the MWI scatter plots of all three α-Syn pathological mutants show events exceeding the ~30 nm boundary, and A30P also shows a high proportion of events exceeding the ~100 pN boundary.

Discussion

Conformational equilibria of α-Syn variants in the 3S3 construct

Ensemble-averaged experiments and spectroscopies have recently been providing experimental evidence of the conformational diversity of NUPs in solution.[50,51] Specifically, several previous works described monomeric α-Syn as exploring different conformations in solution prior to the formation of insoluble fibrils.[9,18,23,27,29,52] In spite of the fact that α-Syn pathogenic mutants have markedly different membrane-permeabilization properties, aggregation behaviors, and toxicities, correspondingly marked differences have not been detected so far in their properties at the monomeric level by mean of bulk experiments. According to this observation, Fredenburg et al. postulated that (as yet unknown) extrinsic factors could contribute to the toxicity of α-Syn in cells, and that the inherent characteristics of monomeric α-Syn mutants are of limited relevance in determining their in vivo properties.[18]

In contrast, the mechanical unfolding data at the single-molecule level we present here show marked differences between WT α-Syn and each of its pathogenic mutants. In particular, mutations were found to affect the monomeric conformational equilibria of the α-Syn variant moieties with respect to both the amount of β-like structuring (Figure 2) and the formation of MWIs (Figure 3). On the other hand, since we detected those differences not in the behavior of free α-Syn in dilute solutions, but in an α-Syn moiety inserted into 3S3 chimeric multimodular constructs, the question arises whether these differences are representative of the effect that mutations have on free monomeric α-Syn.

The presence of I27 linkers could have several plausible repercussions on the behavior of the central α-Syn module. The mere presence of such large objects linked to both termini of α-Syn could give rise to entropic pulling effects, in turn leading to on average more-extended α-Syn conformations. "Aspecific" interactions of the I27 linkers with α-Syn are also plausible. We recently substantiated by CD spectroscopy[30] that the presence of I27 domains in 3S3 construct slightly increases the α-helical content of the central α-Syn. I27 linkers could also give rise to "crowding effects".[53–56] Since six I27 modules are present for each α-Syn, the volume left accessible to α-Syn conformational changes is severely limited. The effect of macromolecular crowding on α-Syn aggregation properties is well characterized.[57–59] Molecular crowding gives rise to excluded-volume effects, which promote reactions with negative activation volumes, such as molecular compactions and aggregations. Consequently, α-Syn compact conformations should be more stable and have significantly longer lifetimes in our 3S3 constructs than in α-Syn dissolved in ideal uncrowded solutions, thus leading us to detect a substantially larger amount of α-Syn structured conformers. Intriguingly, the populations we estimated are in good agreement with data on monomeric α-Syn obtained under conditions with high crowding or high α-Syn concentration.[9,12,20] Of course, the fact that the I27 modules are covalently linked to both termini of α-Syn, rather than floating in solution, introduces further effects than simple crowding, as is often the case in natural or chimeric multimodular proteins,[32,54,60] whose contribution to the final observed conformer population is not easy to discern at the moment.

Even considering the above, the crucial observation is that, in all the 3S3 constructs, both WT α-Syn and the mutant moieties are inserted in the same stereochemical context. All 3S3 constructs are identical, except for the relevant α-Syn point mutations. We can therefore attribute the differences observed in the relative abundance of conformational classes to the effect that these mutations have on free monomeric α-Syn, regardless of how exactly the effects described previously modify the conformational equilibria of α-Syn whenever it is included in the 3S3 construct.

The unfolding signals of the mechanically weak interactions correspond to a large variety of conformations

While each set of 3S3 unfolding curves assigned to random and β-like-containing α-Syn conformations is remarkably homogenous within the set, a more complex multiplicity of conformations results from the measured unfolding distances and forces of weak peaks. Further experiments would be necessary to univocally assign these signals to specific α-Syn conformations. The possibility exists that parts of these signals are due to interactions between the central α-Syn moiety and flanking I27 modules, as we discussed recently.[30] One class of conformers that could be compatible with the observed weak α-Syn unfolding signals is represented by those conformations that have an incomplete β structure. Possible "pre-β" structures are in equilibrium with the fully formed β structure found in curves with seven peaks, and en route to either acquiring or losing that structure. This hypothesis is strengthened by the observation that there is an inverse proportion between the population of MWI and β structures (Figure 2B). On this basis, since weak signals originating from A30P have on average higher rupture forces than those showed by WT and by the other two mutants, the "pre-β" conformations are mechanically

more stable for this mutant, and therefore possibly more structured.

Bertoncini et al. demonstrated that the two mutants A30P and A53T show weaker average signals from long-range interactions than the WT protein, as measured by NMR residual dipolar coupling and paramagnetic relaxation enhancement measurements.[28] This is in agreement with the result presented here of a substantially decreased fraction of detected MWIs (around ~20%) in the A30P and A53T mutant samples, in contrast to the ~50% displayed by the wild-type. Moreover the same study showed that mutant proteins are more flexible and able to sample a larger range of conformations; this agrees with our measurements of an increased variety of lengths associated with their MWI signals (Figure 3). It would be interesting to see by NMR experiments similar to those of Bertoncini et al. if, in the mutant E46K, long-range interactions are more conserved with respect to the A30P and A53T mutants, as suggested by its larger population of conformers displaying MWI.

Conclusions

The effects of the single-point mutations responsible for familial PD on the conformational equilibria of monomeric α-Syn were evaluated. The mutations were found to shift the equilibria towards more-structured conformers. Since the oligomerization step is likely to be the one most directly influenced by the monomeric conformational equilibrium, it would be tempting to propose the hypothesis that the perturbations we found in the equilibria, and in particular the increase of structure in the monomer, are linked to the propensity to form oligomers. However, since the characterization of α-Syn oligomers is still sparse in literature, we cannot currently trace a direct, quantitative correlation between our monomeric data and the propensity of an α-Syn mutant to form a specific class of oligomeric intermediates. A more detailed knowledge of the α-Syn oligomerization process, detailing its relationship with the conformational properties of the monomers, will be necessary to substantiate this correlation. Systematic studies on oligomerization are just beginning to appear in literature.[13,61]

All the conceivable α-Syn aggregation processes, including the formation of any type of oligomer and fibril, require the progressive increase of α-Syn structure, with a substantial prevalence of β-sheet structured forms.[6,12] The increased population of β-sheet conformers shown by the mutants, and their access to longer-range MWIs (Figures 2A and 3) imply more globular structures with an increased number of attractive self-interactions that significantly differ from the WT. This increase can explain the higher propensity to form both oligomeric and polymeric structures.[23] In accord with this hypothesis, even though there are differences in their individual fibrillization and oligomerization properties, all three mutants show an accelerated monomer consumption rate with respect to WT α-Syn, as evidenced by the in-bulk fibrillization kinetics experiments so far reported by different authors.[18,19]

Experimental Section

Polyprotein design and expression: The protocol closely follows the one described in ref. [30]. We reproduced the protein construct design proposed by J. Fernandez for the study of the random coiled Titin N2B segment.[62] Chimeric polyproteins were obtained from pAFM1–4, pAFM5–8 vectors, kindly provided by Prof. Jane Clarke (Cambridge University, UK) and constructed according to ref. [63]. α-Syn or its point-mutated sequences were amplified by PCR by using a couple of primers containing KpnI and XbaI restriction sites. The original eight I27 module plasmid was reconstituted from pAFM1–4 and pAFM5–8, obtaining the pAFM8m vector. pAFM8m was then digested with KpnI and XbaI and ligated to the amplified α-Syn sequence cleaved by the same enzymes to give the pAFM3s3 vector (see ref. [30]). The obtained expression plasmids code for four chimeric polyproteins containing a single α-Syn module (WT, A30P, A53T, or E46K) flanked on either side by three tandem I27 domains, collectively named 3S3. Vectors were transformed into *Escherichia coli* C41(DE3) cells[64] (obtained from Prof. John E. Walker, Medical Research Council–Dunn Human Nutrition Unit, Cambridge, UK, with the agreement of the Medical Research Council Center of Cambridge). The cells were grown, and the expression of proteins was induced as described in ref. [63]. Recombinant proteins were purified by Ni^{2+} affinity chromatography in sodium phosphate buffer (20 mM, pH 8, 500 mM NaCl); the elution from the resin was obtained with imidazole (20 mM). After dialysis, the proteins were kept at −80 °C in phosphate buffered saline (PBS) with 30% glycerol.

Buffer elemental analysis: Due to the well-known structuring effects of divalent metal ions on α-Syn,[65] an accurate elemental analysis of the buffer was performed to exclude artifacts in our results arising from metal contamination. A Tris/HCl buffer solution (500 mM, pH 7.5) was analyzed for metal contents by atomic absorption spectroscopies. The measured concentrations were Cu = 0.2 ± 0.1 nM, Zn = 3.5 ± 0.1 nM, Fe = 0.9 ± 0.1 nM, and Ca = 22.5 ± 0.1 nM. These values are two orders of magnitude lower than the concentration required to induce structural effects on α-Syn.[66]

Surface preparation: We followed the template-stripped gold (TSG) surface preparation described by Wagner et al.[67,68] Briefly, gold (Alfa Aesar, 99.99%) was deposited onto freshly cleaved mica substrates (Mica New York Corp., clear ruby muscovite) in a high-vacuum evaporator (Denton Vacuum, model DV502A) at 10^{-5} Torr. Before deposition, the mica was preheated to 350 °C by a heating stage mounted behind it to enhance the formation of terraced Au(111) domains. The typical evaporation rate was 3 Å s^{-1}, and the thickness of the gold films ranged around 300 nm. The mica temperature was maintained at 350 °C for 2 h after deposition for annealing. This method produced samples with flat Au(111) terraces. These films were fixed to a glass substrate with EPO-TEK 377 (Epoxy Tech, Billerica, MA, USA). They were then separated at the gold–mica interface by peeling immediately before functionalization with the desired molecules. This procedure produced gold substrates with a flat surface morphology due to the templating effect of the atomically flat mica surface.[67,68]

SMFS experiments: For each experiment, a drop of the chosen 3S3 construct solution (20 μL, ~100 μg mL^{-1}) was deposited on the freshly peeled gold surface for about 20 min. SMFS experiments were performed by using a commercially available AFM system: Picoforce AFM with Nanoscope IIIa controller (Digital Instruments, Plainview, NY, USA) using V-shaped silicon nitride cantilevers (NP; Digital Instruments) with a spring constant calibrated by the thermal noise method.[69] The pulling speed was 2.18 μm s^{-1} for all ex-

periments. The buffer used was Tris/HCl (10 mM, pH 7.5). To assess the statistical validity of the comparison between data obtained with different 3S3 constructs, standard χ^2 tests were performed. The differences between data sets are significant with $p < 0.01$, the exception being represented by one pair of mutants, whose differences are less likely to be statistically significant (see Table S1).

Data analysis: The force curves were analyzed by using Hooke, an open-source force spectroscopy data analysis program available at http://code.google.com/p/hooke (M.S. et al., unpublished results). Mechanical unfolding peaks were fitted with a worm-like chain force versus extension model[70] with two free parameters [Eq. (1)]: contour length (L) and persistence length (p). Due to fit instability, the smaller MWIs have instead been fitted with only the L parameter free, and p fixed at 0.35 nm. Peaks were characterized in terms of the length of the polypeptide chain extended after each unfolding event by comparing the fitted WLC contour lengths of successive peaks.

$$F = \frac{k_b T}{p}\left(\frac{x}{L} + {}^1\!/_4\left(1-\frac{x}{L}\right)^{-2} - {}^1\!/_4\right) \quad (1)$$

Curve selection and classification: Only those force curves attributable to the complete mechanical unfolding of a single 3S3 construct were chosen. First, the raw data output of the instrument was automatically filtered by the Hooke software, discarding the curves that contained fewer than four force peaks on the retraction trace. The peaks are recognized by means of a simple convolution algorithm (see the Hooke documentation and source code online for details). This ensures that curves containing no or only a few force peaks (usually about 90% of the total) are not considered for analysis.

The remaining curves were then analyzed by the operator in two review iterations. In the first step, the set of curves was visually reviewed and annotated by the operator, taking note of the number of peaks and of any noteworthy features of the force curve. This review helps to pinpoint the curves more likely to belong to the unfolding of a single 3S3 molecule and to notice repeatable patterns. In the second iteration, curves were reviewed taking note of the number of peaks, initial and final contour length, and overall appearance, and only the ones that fit the expected unfolding pattern of a single 3S3 molecule (with respect to the total length, number of peaks, peak force hierarchy, contour length increase upon domain unfolding, rupture forces, etc.) were chosen for the final statistics. Curves corresponding to the unfolding of a whole 3S3 molecule but in which the first part of the curve was substantially obscured by aspecific forces were also discarded. The remaining curves (about 0.5–0.1% of the original sample) were found to belong to three kinds of reproducible patterns, corresponding to the three classes described in this paper. To avoid excessive operator bias, the first and second review iterations were performed and/or checked by different operators.

Acknowledgements

We thank Dr. J. Clarke for kindly providing the vectors for constructs expression, Professor J. E. Walker for supplying us with the E. coli *C41(DE3) cells and Prof. Mark Cookson (NIH, Bethesda) for cDNA coding for mutated α-Syn sequences. This work was supported by the Ministero dell'Università e della Ricerca–Fondo per gli Investimenti della Ricerca di Base (MIUR-FIRB) RBNE03PX83/001; MIUR-FIRB Progetto NG-lab (G.U. 29/07/05 n.175); EU FP6-STREP program NMP4-CT-2004-013775 NUCAN. L.B. is also supported by PRIN 2005 and FIRB ProgettoRBNE03PX83/006.*

Keywords: AFM · aggregation · alpha-synuclein · Parkinson's disease · single-molecule studies

[1] M. Windisch, H. Wolf, B. Hutter-Paier, R. Wronski, *Neurodegener. Dis.* **2008**, *5*, 218.
[2] A. I. Tröster, *Neuropsychol. Rev.* **2008**, *18*, 103.
[3] V. N. Uversky, *J. Neurochem.* **2007**, *103*, 17.
[4] M. Vilar, H. T. Chou, T. Luhrs, S. K. Maji, D. Riek-Loher, R. Verel, G. Manning, H. Stahlberg, R. Riek, *Proc. Natl. Acad. Sci. USA* **2008**, *105*, 8637.
[5] Z. Qin, D. Hu, S. Han, D. P. Hong, A. L. Fink, *Biochemistry* **2007**, *46*, 13322.
[6] V. N. Uversky, *J. Biomol. Struct. Dyn.* **2003**, *21*, 211.
[7] P. Tompa, *FEBS Lett.* **2005**, *579*, 3346.
[8] V. N. Uversky, *Curr. Alzheimer Res.* **2008**, *5*, 260.
[9] J. C. Lee, R. Langen, P. A. Hummel, H. B. Gray, J. R. Winkler, *Proc. Natl. Acad. Sci. USA* **2004**, *101*, 16466.
[10] H. A. Lashuel, B. M. Petre, J. Wall, M. Simon, R. J. Nowak, T. Walz, P. T. Lansbury, *J. Mol. Biol.* **2002**, *322*, 1089.
[11] N. C. Maiti, M. M. Apetri, M. G. Zagorski, P. R. Carey, V. E. Anderson, *J. Am. Chem. Soc.* **2004**, *126*, 2399.
[12] M. M. Apetri, N. C. Maiti, M. G. Zagorski, P. R. Carey, V. E. Anderson, *J. Mol. Biol.* **2006**, *355*, 63.
[13] K. M. Danzer, D. Haasen, A. R. Karow, S. Moussaud, M. Habeck, A. Giese, H. Kretzschmar, B. Hengerer, M. Kostka, *J. Neurosci.* **2007**, *27*, 9220.
[14] T. T. Ding, S. J. Lee, J. C. Rochet, P. T. Lansbury, *Biochemistry* **2002**, *41*, 10209.
[15] D. E. Ehrnhoefer, J. Bieschke, A. Boeddrich, M. Herbst, L. Masino, R. Lurz, S. Engemann, A. Pastore, E. E. Wanker, *Nat. Struct. Mol. Biol.* **2008**, *15*, 558.
[16] M. J. Volles, S. J. Lee, J. C. Rochet, M. D. Shtilerman, T. T. Ding, J. C. Kessler, P. T. Lansbury, *Biochemistry* **2001**, *40*, 7812.
[17] H. A. Lashuel, D. Hartley, B. M. Petre, T. Walz, P. T. Lansbury, *Nature* **2002**, *418*, 291.
[18] R. A. Fredenburg, C. Rospigliosi, R. K. Meray, J. C. Kessler, H. A. Lashuel, D. Eliezer, P. T. Lansbury, *Biochemistry* **2007**, *46*, 7107.
[19] K. A. Conway, S. J. Lee, J. C. Rochet, T. T. Ding, R. E. Williamson, P. T. Lansbury, *Proc. Natl. Acad. Sci. USA* **2000**, *97*, 571.
[20] J. Li, V. N. Uversky, A. L. Fink, *Neurotoxicology* **2002**, *23*, 553.
[21] W. Choi, S. Zibaee, R. Jakes, L. C. Serpell, B. Davletov, R. A. Crowther, M. Goedert, *FEBS Lett.* **2004**, *576*, 363.
[22] T. Kamiyoshihara, M. Kojima, K. Ueda, M. Tashiro, S. Shimotakahara, *Biochem. Biophys. Res. Commun.* **2007**, *355*, 398.
[23] S. Krishnan, E. Y. Chi, S. J. Wood, B. S. Kendrick, C. Li, W. Garzon-Rodriguez, J. Wypych, T. W. Randolph, L. O. Narhi, A. L. Biere, M. Citron, J. F. Carpenter, *Biochemistry* **2003**, *42*, 829.
[24] K. A. Conway, S. J. Lee, J. C. Rochet, T. T. Ding, J. D. Harper, R. E. Williamson, P. T. J. Lansbury, Jr., *Ann. N. Y. Acad. Sci.* **2000**, *920*, 42.
[25] H. J. Koo, H. J. Lee, H. Im, *Biochem. Biophys. Res. Commun.* **2008**, *368*, 772.
[26] E. A. Greenbaum, C. L. Graves, A. J. Mishizen-Eberz, M. A. Lupoli, D. R. Lynch, S. W. Englander, P. H. Axelsen, B. I. Giasson, *J. Biol. Chem.* **2005**, *280*, 7800.
[27] R. Bussell, D. Eliezer, *J. Biol. Chem.* **2001**, *276*, 45996.
[28] C. W. Bertoncini, C. O. Fernandez, C. Griesinger, T. M. Jovin, M. Zweckstetter, *J. Biol. Chem.* **2005**, *280*, 30649.
[29] E. Palecek, V. Ostatna, M. Masarik, C. W. Bertoncini, T. M. Jovin, *Analyst* **2008**, *133*, 76.
[30] M. Sandal, F. Valle, I. Tessari, S. Mammi, E. Bergantino, F. Musiani, M. Brucale, L. Bubacco, B. Samorì, *PLoS Biol.* **2008**, *6*, e6.
[31] C. Bustamante, Y. R. Chemla, N. R. Forde, D. Izhaky, *Annu. Rev. Biochem.* **2004**, *73*, 705.
[32] J. H. Han, S. Batey, A. A. Nickson, S. A. Teichmann, J. Clarke, *Nat. Rev. Mol. Cell Biol.* **2007**, *8*, 319.
[33] B. Samorì, G. Zuccheri, P. Baschieri, *ChemPhysChem* **2005**, *6*, 29.
[34] A. F. Oberhauser, M. Carrion-Vazquez, *J. Biol. Chem.* **2008**, *283*, 6617.

[35] M. Carrion-Vazquez, A. F. Oberhauser, T. E. Fisher, P. E. Marszalek, H. Li, J. M. Fernandez, *Prog. Biophys. Mol. Biol.* **2000**, *74*, 63.
[36] T. E. Fisher, A. F. Oberhauser, M. Carrion-Vazquez, P. E. Marszalek, J. M. Fernandez, *Trends Biochem. Sci.* **1999**, *24*, 379.
[37] A. F. Oberhauser, P. K. Hansma, M. Carrion-Vazquez, J. M. Fernandez, *Proc. Natl. Acad. Sci. USA* **2001**, *98*, 468.
[38] B. Samorì, *Chem. Eur. J.* **2000**, *6*, 4249.
[39] F. Grandi, M. Sandal, G. Guarguaglini, E. Capriotti, R. Casadio, B. Samorì, *ChemBioChem* **2006**, *7*, 1774.
[40] M. Sandal, F. Grandi, B. Samorì, *Polymer* **2006**, *47*, 2571.
[41] F. Valle, M. Sandal, B. Samorì, *Phys. Life Rev.* **2007**, *4*, 157.
[42] H. Dietz, M. Bertz, M. Schlierf, F. Berkemeier, T. Bornschlogl, J. P. Junker, M. Rief, *Nat. Protocols* **2006**, *1*, 80.
[43] H. Dietz, M. Rief, *Proc. Natl. Acad. Sci. USA* **2006**, *103*, 1244.
[44] M. Rief, M. Gautel, H. E. Gaub, *Elastic Filaments Cell, 2000* **2000**, *481*, 129.
[45] S. Kasas, G. Dietler, *Pfluegers Arch.* **2008**, *456*, 13.
[46] M. Favre, L. A. Chtcheglova, D. A. Lapshin, S. K. Sekatskii, F. Valle, G. Dietler, *Ultramicroscopy* **2007**, *107*, 882.
[47] B. A. Smith, D. A. Anselmetti, *Abstr. Pap. Am. Chem. Soc.* **2001**, *221*, U344.
[48] A. Borgia, P. M. Williams, J. Clarke, *Annu. Rev. Biochem.* **2008**, *77*, 101.
[49] A. F. Oberhauser, P. E. Marszalek, M. Carrion-Vazquez, J. M. Fernandez, *Nat. Struct. Biol.* **1999**, *6*, 1025.
[50] F. Zhu, J. Kapitan, G. E. Tranter, P. D. Pudney, N. W. Isaacs, L. Hecht, L. D. Barron, *Proteins Struct. Funct. Bioinf.* **2008**, *70*, 823.
[51] M. von Bergen, S. Barghorn, S. Jeganathan, E. M. Mandelkow, E. Mandelkow, *Neurodegener. Dis.* **2006**, *3*, 197.
[52] R. C. Rivers, J. R. Kumita, G. G. Tartaglia, M. M. Dedmon, A. Pawar, M. Vendruscolo, C. M. Dobson, J. Christodoulou, *Protein Sci.* **2008**, *17*, 887.
[53] A. P. Minton, *Curr. Opin. Struct. Biol.* **2000**, *10*, 34.
[54] S. Batey, J. Clarke, *J. Mol. Biol.* **2008**, *378*, 297.
[55] A. S. Morar, A. Olteanu, G. B. Young, G. J. Pielak, *Protein Sci.* **2001**, *10*, 2195.
[56] B. C. McNulty, G. B. Young, G. J. Pielak, *J. Mol. Biol.* **2006**, *355*, 893.
[57] L. A. Munishkina, A. Ahmad, A. L. Fink, V. N. Uversky, *Biochemistry* **2008**, *47*, 8993.
[58] V. N. Uversky, E. M. Cooper, K. S. Bower, J. Li, A. L. Fink, *FEBS Lett.* **2002**, *515*, 99.
[59] M. D. Shtilerman, T. T. Ding, P. T. Lansbury, *Biochemistry* **2002**, *41*, 3855.
[60] S. Batey, L. G. Randles, A. Steward, J. Clarke, *J. Mol. Biol.* **2005**, *349*, 1045.
[61] K. C. Luk, E. G. Hyde, J. Q. Trojanowski, V. M. Y. Lee, *Biochemistry* **2007**, *46*, 12522.
[62] H. Li, W. A. Linke, A. F. Oberhauser, M. Carrion-Vazquez, J. G. Kerkvliet, H. Lu, P. E. Marszalek, J. M. Fernandez, *Nature* **2002**, *418*, 998–1002.
[63] A. Steward, J. L. Toca-Herrera, J. Clarke, *Protein Sci.* **2002**, *11*, 2179.
[64] B. Miroux, J. E. Walker, *J. Mol. Biol.* **1996**, *260*, 289.
[65] V. N. Uversky, J. Li, A. L. Fink, *J. Biol. Chem.* **2001**, *276*, 44284.
[66] A. Binolfi, R. M. Rasia, C. W. Bertoncini, M. Ceolin, M. Zweckstetter, C. Griesinger, T. M. Jovin, C. O. Fernandez, *J. Am. Chem. Soc.* **2006**, *128*, 9893.
[67] M. Hegner, P. Wagner, G. Semenza, *Surf. Sci.* **1993**, *291*, 39.
[68] P. Wagner, M. Hegner, H. J. Guntherodt, G. Semenza, *Langmuir* **1995**, *11*, 3867.
[69] E. L. Florin, M. Rief, H. Lehmann, M. Ludwig, C. Dornmair, V. T. Moy, H. E. Gaub, *Biosens. Bioelectron.* **1995**, *10*, 895.
[70] C. Bustamante, J. F. Marko, E. D. Siggia, S. Smith, *Science* **1994**, *265*, 1599.

Received: August 28, 2008
Published online on December 9, 2008

